

Conical Winds from the Disk-Magnetosphere Boundary

M. M. Romanova,^{1*}, G. V. Ustyugova^{2†}, A. V. Koldoba^{3‡}, R. V. E. Lovelace^{1,4§}

¹ Department of Astronomy, Cornell University, Ithaca, NY 14853, USA

² Keldysh Institute of Applied Mathematics, Russian Academy of Sciences, Moscow, Russia

³ Institute of Mathematical Modeling, Russian Academy of Sciences, Moscow, Russia

⁴ Department of Applied and Eng. Phys., Cornell University, Ithaca, NY 14853

21 July 2021

ABSTRACT

A new type of wind - a conical wind - has been discovered in axisymmetric magneto-hydrodynamic simulations of the disk-magnetosphere interaction in cases where the magnetic field of the star is bunched into an X-type configuration. Such a configuration arises if the effective viscosity of the disk is larger than the effective diffusivity, or if the accretion rate in the disk is enhanced. Conical outflows flow from the inner edge of the disk into a narrow shell with half-opening angle of $30 - 45^\circ$. The outflow carries $\sim 0.1 - 0.3$ of the disk mass accretion rate and part of the disk's angular momentum. The conical winds are driven by the gradient of the magnetic pressure which exists above the disk due to the winding of the stellar magnetic field. Exploratory 3D simulations show that conical winds are symmetric about rotation axis of the disk even if the magnetic dipole is significantly misaligned with the disk's rotation axis. Conical winds appear around stars of different periods. However, in the case of a star in the “propeller” regime, an additional - much faster component appears: an axial jet, where matter is accelerated up to very high velocities at small distances from the star by magnetic pressure force above the surface of the star. The simulations are done in dimensionless units and are applicable to a variety of the disk-accreting magnetized stars: young stars, white dwarfs, neutron stars, and possibly black holes. For the case of young stars, conical winds and axial jets may appear in different cases, including Class I young stars, classical T Tauri stars, and EXors. In EXors periods of enhanced accretion may lead to the formation of conical winds which correspond to the outflows observed from these stars.

Key words: accretion, accretion discs; MHD; stars: magnetic fields

1 INTRODUCTION

Jets and winds are observed in many objects from young stars to systems with white dwarfs, neutron stars, and black holes (e.g., Livio 1997). For example, jets have recently been observed from the accreting neutron star Circinus X-1 (Heinz et al. 2007). The jet shows a conical structure with a half-opening angle about 30° . This conical structure could be explained by precession of the jet. However, 10 years of observations show that orientation of the jet has not changed (Tudose et al. 2008). Jets and outflows are also observed from symbiotic stars where matter flows from the vicinity of white dwarfs during periods of enhanced accretion (e.g., Sokoloski & Kenyon 2003). It is often the case that outflows are as-

sociated with enhanced accretion (e.g., Cabrit et al. 1990; Lovelace, Romanova, Newman 1994).

A large body of observations has been accumulated on outflows from young stars at different stages of their evolution from very young stars where powerful jets are observed up to classical T Tauri stars (CTTSs) where weaker jets and winds are observed (see review by Ray et al. 2007). A significant number of CTTS show signs of outflows in spectral lines, in particular in He I (Edwards et al. 2006; Kwan, Edwards, & Fischer 2007). High-resolution observations show that outflows often have an “onion-skin” structure, with high-velocity outflows in the axial region, and lower-velocity outflow at larger distance from the axis (Bacciotti et al. 2000). High angular resolution spectra of $[\text{FeII}]\lambda 1.644\mu\text{m}$ emission line taken along the jets of DG Tau, HL Tau and RW Auriga reveal two components: a high-velocity well-collimated extended component with velocity $v \sim 200 - 400$ km/s and a low-velocity $v \sim 100$ km/s uncollimated component which is close to the star (Pyo et al. 2003, 2006). High-resolution

* E-mail: romanova@astro.cornell.edu

† E-mail: ustyugg@rambler.ru

‡ E-mail: koldoba@rambler.ru

§ E-mail: lovelace@astro.cornell.edu

observations of molecular hydrogen in HL Tau have shown that at small distances from the star the flow shows a conical structure with outflow velocity $\sim 50 - 80$ km/s (Takami et al. 2007). EXors represent an interesting stage of evolution of young stars where enhanced accretion leads to period of enhanced outflows (e.g., Brittain et al. 2007)

Different models have been proposed to explain outflows from CTTSs (see review by Ferreira, Dougados, & Cabrit 2006). The models include those where the outflow originates from a radially distributed disk wind (Königl & Pudritz 2000; Ferreira et al. 2006) or from the innermost region of the accretion disk (e.g., Lovelace, Berk & Contopoulos 1991; Livio 1997). Further, there is the X-wind model (Shu et al. 1994; 2007; Najita & Shu 1994; Cai et al. 2008) where most of the matter outflows from the disk-magnetosphere boundary. This work focuses on the outflows from the inner part of the disk or disk-magnetosphere boundary. We discovered conditions which favor conical outflows and performed axisymmetric and exploratory 3D MHD simulations for both slowly and rapidly rotating stars including stars in the propeller regime.

Earlier we investigated outflows from accreting rapidly-rotating magnetized stars in the “propeller” regime (e.g., Il-larionov & Sunyaev 1975; Lovelace, Romanova & Bisnovaty-Kogan 1999; Alpar & Shaham 1985) where the magnetosphere rotates faster than the inner regions of the disk and the magnetosphere transfers its angular momentum to the disk matter (e.g. Lovelace et al. 1999). Simulations show that most of matter flows from the inner parts of the disk to wide-angle open cones. At the same time most of the angular momentum and rotational energy of the star outflows along open stellar magnetic field lines in a collimated, magnetically dominated jet of low-density and high-velocity (Romanova et al. 2005; Ustyugova et al. 2006).

In the present study we were able to obtain conical winds in cases of *slowly* rotating stars, where new disk matter arrives after period of lower accretion. In this situation the poloidal field lines are bunched into an X-type configuration and persistent conical winds are observed. Compared to X-winds proposed earlier by Shu and collaborators (e.g. Shu et al. 1994) conical winds are strongly non-stationary and they may originate from a star with any rotation rate. Such winds may appear and blow during periods of enhanced accretion, or may appear in any situation where the inward accretion velocity of the disk is higher than outward diffusion of the magnetic field. Simulations were done in dimensionless form and such winds may appear around magnetized stars of different sizes from young stars to neutron stars, and also possibly around magnetized black holes.

In §2 we describe the model. In §3 we describe the physics of conical outflows. In §4 we discuss dependence of the results on different parameters. In §5 we show exploratory 3D simulations of conical outflows. In §6 we discuss application of the model to EXors and CTTSs. In §7 we compare conical winds with propeller-driven winds and other types of winds. In §8 we present discussion and conclusions.

2 MODEL

We have done axisymmetric and exploratory 3D MHD simulations of the interaction of an accretion disk with the magnetosphere of a rotating star. The corotation radius of the star

	CTTSs	White dwarfs	Neutron stars
$M(M_\odot)$	0.8	1	1.4
R	$2R_\odot$	5000 km	10 km
R_0 (cm)	2.8×10^{11}	1.0×10^9	2×10^6
v_0 (cm s $^{-1}$)	1.95×10^7	3.6×10^8	9.7×10^9
ω_0 (s $^{-1}$)	2.0×10^{-4}	0.36	4.8×10^3
P_0	1.04 days	17.2 s	1.3 ms
B_{*0} (G)	10^3	10^6	10^9
B_0 (G)	100	1.2×10^4	1.2×10^7
ρ_0 (g cm $^{-3}$)	4.1×10^{-13}	3.7×10^{-8}	1.7×10^{-6}
n_0 (1/cm $^{-3}$)	2.4×10^{11}	7.0×10^{14}	1.0×10^{18}
$\dot{M}_0(M_\odot \text{yr}^{-1})$	2.0×10^{-8}	1.3×10^{-8}	2.0×10^{-9}

Table 1. Sample reference values of the dynamical quantities used in our simulations.

$r_{cr} = (GM_*/\Omega_*^2)^{1/3}$ is in most cases larger than the magnetospheric radius r_m which is determined by the balance between the pressure of the star’s magnetic field and the ram pressure of the disk matter.

The model we use is similar to that described in Romanova et al. (2005) and Ustyugova et al. (2006). Specifically, (1) a spherical coordinate system (r, θ, ϕ) is used which gives high grid resolution near the dipole; (2) the complete set of MHD equations is solved to find the eight variables $(\rho, v_R, v_\theta, v_\phi, B_r, B_\theta, B_\phi, \epsilon)$ (with ϵ the specific internal energy); (3) a Godunov-type numerical method is used; (4) an effective viscosity and effective magnetic diffusivity are incorporated the code using an α -model controlled by dimensionless parameters α_v and α_d . We varied both parameters in the range 0.01 – 1.

2.1. Initial and Boundary Conditions. Initially we suggest that the disk is far away from the star (beyond the external boundary of the simulation region), so that the non-perturbed dipole field of the star initially occupies the entire simulation region and the magnetic field of the star is a dipole: $\mathbf{B} = [3(\boldsymbol{\mu} \cdot \mathbf{r})\mathbf{r} - \boldsymbol{\mu}r^2]/|\mathbf{r}|^5$, where $\boldsymbol{\mu}$ is the star’s magnetic moment. The simulation region is filled with a low-density corona and is initially non-rotating. The corona is isothermal and in thermal equilibrium, so that the density and pressure distributions are: $\rho = \rho_0 \exp[GM/(c_s^2 r)]$ and $p = c_s^2 \rho_0 \exp[GM/(c_s^2 r)]$, where c_s is the isothermal sound speed, ρ_0 is the matter density at the infinity (approximately equal to that on the external boundary). To ensure the gradual start-up (smooth initial conditions) we start to rotate star with very small angular velocity corresponding to the corotation radius at the external boundary $R_{out}, r_{cor} = R_{out}(GM/\Omega_d^2)^{1/3}$ and later gradually increase the angular velocity from that up to much larger values Ω during 10 periods of rotation of the disk at $r = 1$. The (final) angular velocity of the star was different in different runs ranging from very small (corresponding to $r_{cor} = 10$) up to very large (corresponding to $r_{cor} = 1$) with most of runs done at intermediate value $r_{cor} = 3$ (angular velocity of the star in dimensionless units $\Omega_* \approx 0.19$). Spinning-up of the star leads to spinning-up of the magnetosphere and the low-density corona. We checked that rotating dipole brings the corona to corotation in a very short time (with a speed corresponding to propagation of a torsional Alfvén waves through the corona).

We divided the external boundary to the region of corona, $\theta < \theta_{disk}$ and the region of the disk, $\theta > \theta_{disk}$. In the

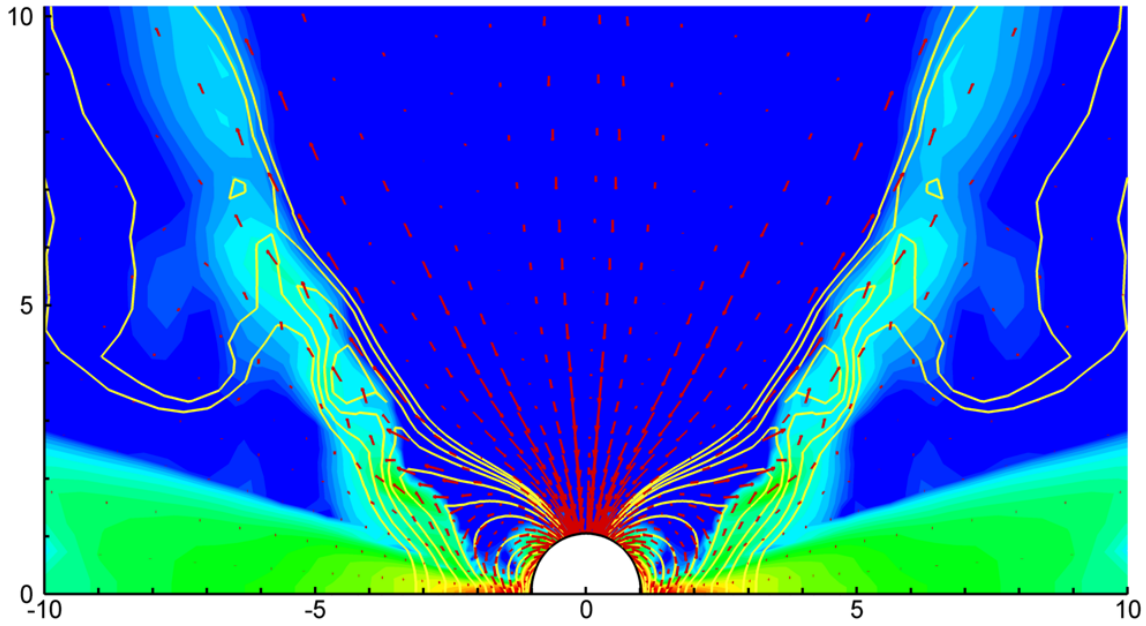


Figure 1. A snapshot of the outflow to conical winds, at the moment of time $T = 500$. The background shows logarithm of the absolute value of the poloidal matter flux, lines are the sample magnetic field lines, and arrows are vectors of the poloidal velocity.

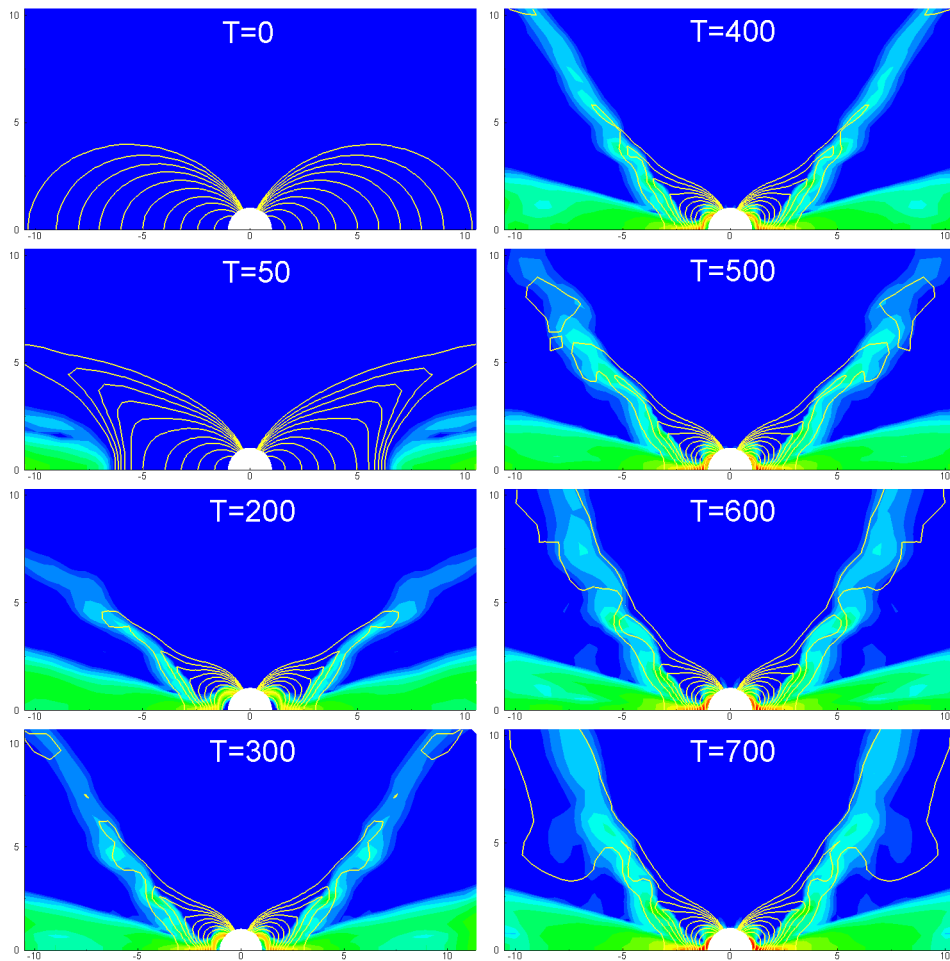


Figure 2. Figure shows formation and evolution of conical winds with time. The background shows logarithm of the absolute value of the poloidal matter flux, lines - are selected magnetic field lines.

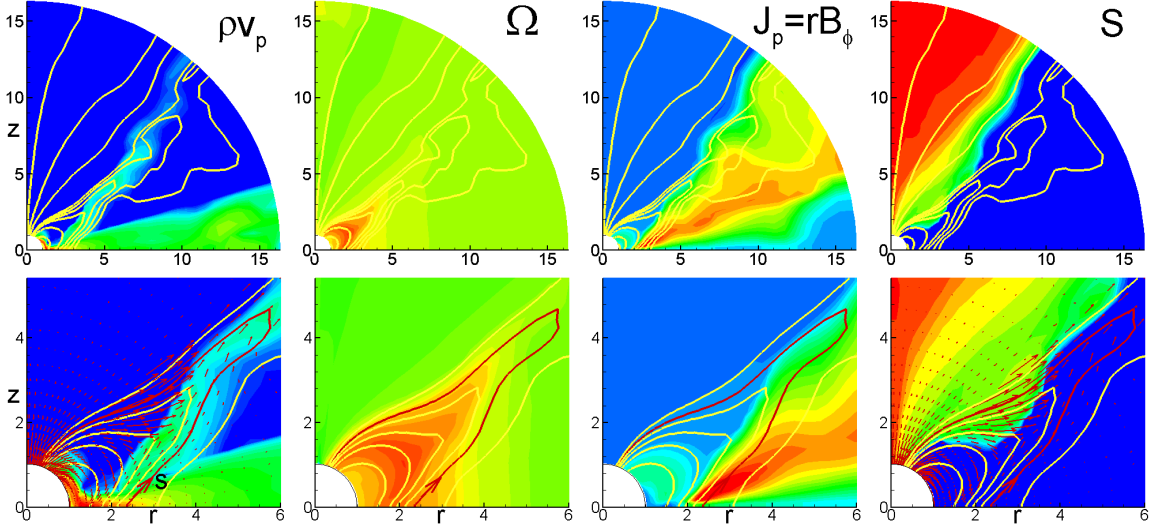


Figure 3. Different values shown for one moment of time, $T = 500$ in the whole region (top panels) and near the star (bottom panels). The background shows (from left to right): the logarithm of the absolute value of the poloidal matter flux, ρv_p , angular velocity, Ω , poloidal current, $J_p = rB_\phi$, and entropy S . Lines are selected magnetic field lines. Thick line is a magnetic field line which is used for analysis of flow in the direction of conical winds. Vectors are velocity vectors. An arrow shows that the distance s along the line used in the subsequent plots starts at the disk.

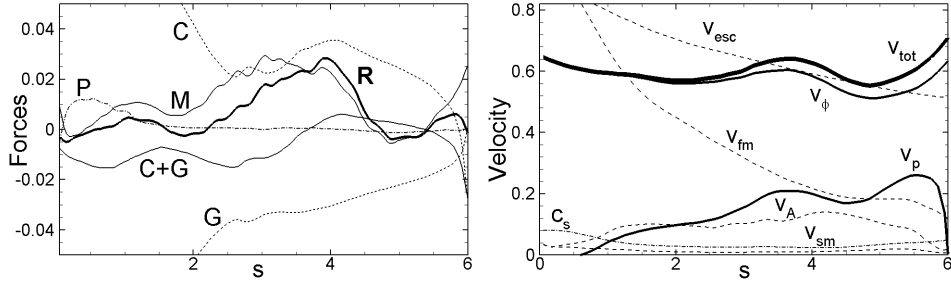


Figure 4. Left panel: Forces along the part of the magnetic field line shown on the Fig. 3 starting from the disk up to the point when the line curves towards the star. Labels are: G-gravitational, C-centrifugal, M-magnetic, P-pressure gradient, and R - resulting forces. Right panel: velocities projected to the same line: v_{tot} - total, v_p - poloidal, v_ϕ - azimuthal, c_s - sound speed, v_A - Alfvén, v_{sm} - slow magnetosonic, v_{fm} - fast magnetosonic, v_{esc} - escape velocities.

corona we take “free” boundary conditions for all variables, but do not permit matter to flow back to the simulation region from the boundary. In the disk region, we fix the density at some value, $\rho = \rho_d$, and establish slightly sub-Keplerian velocity, $\Omega_d = \kappa\Omega(r_d)$, where $\kappa = \sqrt{1 - 0.003}$ so that matter flows into the simulation region through the boundary. When the matter enters the simulation region it continues to flow inward due to the viscosity incorporated in the code. We use an α -type viscosity with viscosity coefficient proportional to α_{vis} . Diffusivity is incorporated into the code with diffusivity coefficient proportional to coefficient α_{dif} . Inflowing matter has zero magnetic flux. The boundary conditions on the equatorial plane and on the rotation axis are symmetric and antisymmetric (see e.g. Ustyugova et al. 2006).

2.2. Reference Units. The MHD equations were solved in dimensionless form so that results can be applicable to stars of different scales, such as to classical T Tauri stars (CTTSs), to accreting white dwarfs, and to neutron stars. We chose a reference mass $M_0 = M_*$ to be typical mass for different types of stars (see Table). The reference radius is twice the radius

of the star, $R_0 = 2R_*$ and the surface magnetic field B_* is different for different types of stars. The reference velocity is $v_0 = (GM_0/R_0)^{1/2}$, the time-scale $t_0 = R_0/v_0$, and the angular velocity $\Omega_0 = 1/t_0$. We measure time in units of the rotational period with Keplerian speed at $r = R_0$: $P_0 = 2\pi t_0$ and in the plots show dimensionless time $T = t/P_0$. Other reference values: the reference density ρ_0 and number density of particles n_0 , the reference accretion rate $\dot{M}_0 = \rho_0 v_0 R_0^2$ and the reference angular momentum flux $\dot{L}_0 = \dot{M}_0 v_0 R_0$. Table 1 shows examples of reference variables for different stars.

We solved the MHD equations for normalized variables: $\tilde{\rho} = \rho/\rho_0$, $\tilde{v} = v/v_0$, $\tilde{B} = B/B_0$, etc. The plots show the normalized variables (with tilda’s implicit). Examples in dimensional variables are given for young stars.

3 PHYSICS OF CONICAL WINDS

Multiple runs were done in the axisymmetric case for a wide variety of parameters. We chose one set of parameters as our main case and describe it in detail. We observed that the con-

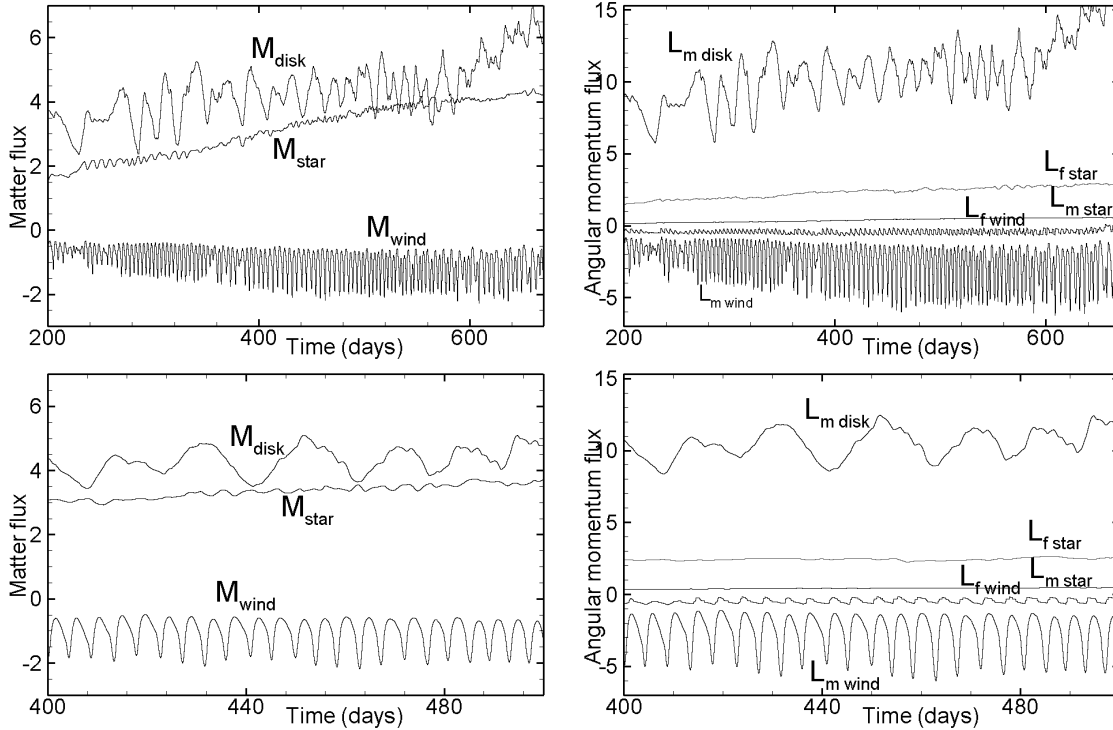


Figure 5. Left panels: matter fluxes to the star \dot{M}_{star} , to conical winds \dot{M}_{wind} and through the disk \dot{M}_{disk} . Right panels: angular momentum fluxes carried by the disk, L_{disk} , to the star carried by matter, L_{mstar} , and by magnetic field, L_{fstar} , and to conical winds, L_{mwinds} and L_{fwinds} . Bottom panels show fluxes during a part of the simulation time.

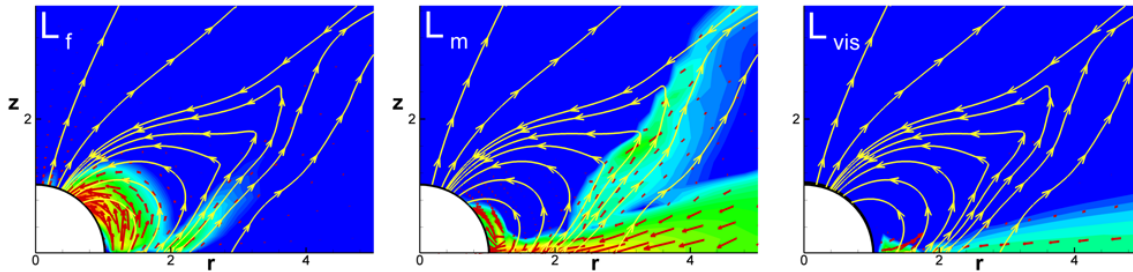


Figure 6. Left panel: the background, vectors and streamlines show angular momentum carried by magnetic field. Middle panel: background and arrows show angular momentum carried by matter, streamlines show angular momentum carried by the field. Right panel: the background shows angular momentum carried by viscosity.

dition $\alpha_{vis} > \alpha_{dif}$ is necessary for conical winds to form. That is, the magnetic Prandtl number of the turbulence, $Pr = \alpha_{vis}/\alpha_{dif} > 1$. In addition, the conical winds are stronger if the diffusivity is not very small, that is if $\alpha_{dif} > 0.03$. Below we show results for $\alpha_{vis} = 0.3$ and $\alpha_{dif} = 0.1$ which we term “the main case”.

For the main case we chose densities in the disk and corona: $\bar{\rho}_d = 10$, $\bar{\rho}_c = 0.001$, corotation radius $\bar{r}_{cor} = 3$. Results can be applied to different types of stars. However, as an example, we show results in dimensional units for typical CTTS, where the reference values are taken from Table 1. For example, for a CTTS with a $\bar{P}_* = 5.4$ days, the unit of time used in figures below is $P_0 = 1.04$ days (see Table, CTTS column).

3.1 Matter flow, velocities and forces

The simulations show that when the disk comes close to the star and bunches the poloidal field lines into an X-type configuration then conical outflows start and continue for a long time, as long as the simulations were run. The Fig. 1 shows a typical view of the matter flow where the matter flux is shown as a background. Matter flows to the cone into a relatively narrow shell and the cone has a half-opening angle, $\theta = 30^\circ - 40^\circ$. The process is non-stationary due to episodes of inflation and reconnection of the magnetic field lines (see animation at <http://www.astro.cornell.edu/~romanova/conical.htm>). One can see that the disk comes quite close to the star. Test simulations (which require much longer runs) have been done for an inner boundary smaller by a factor of two. This showed that the conical winds are similar, while the magnetosphere is larger. The poloidal velocity vectors show that matter is ac-

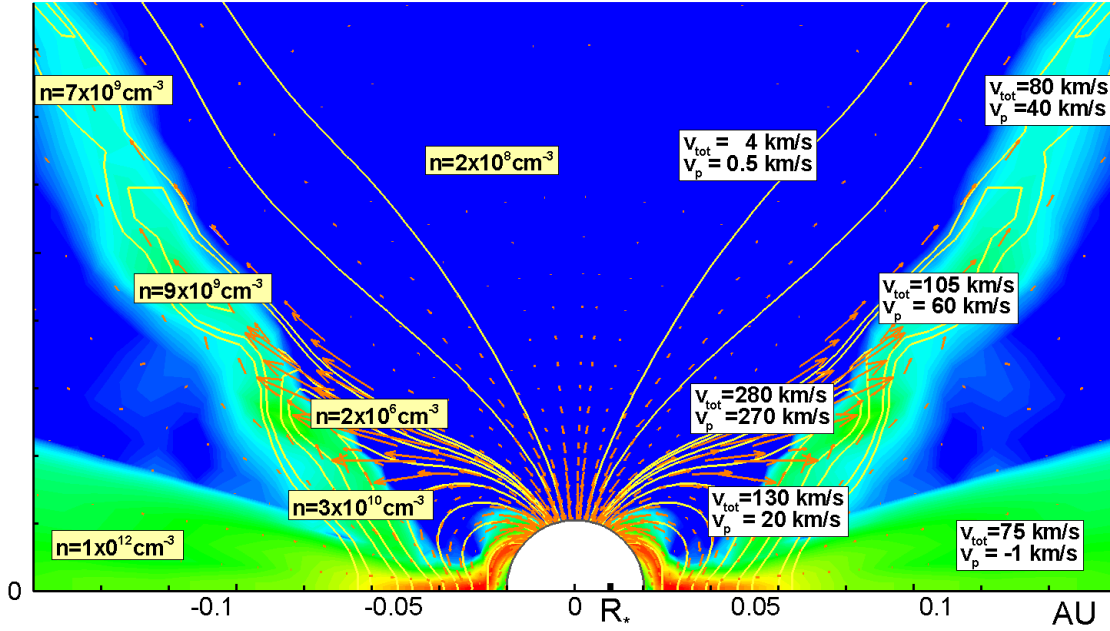


Figure 7. Density and velocity distributions in conical winds for CTTS. Here we converted dimensionless values obtained from simulations to dimensional values for typical T Tauri star taken from the Table.

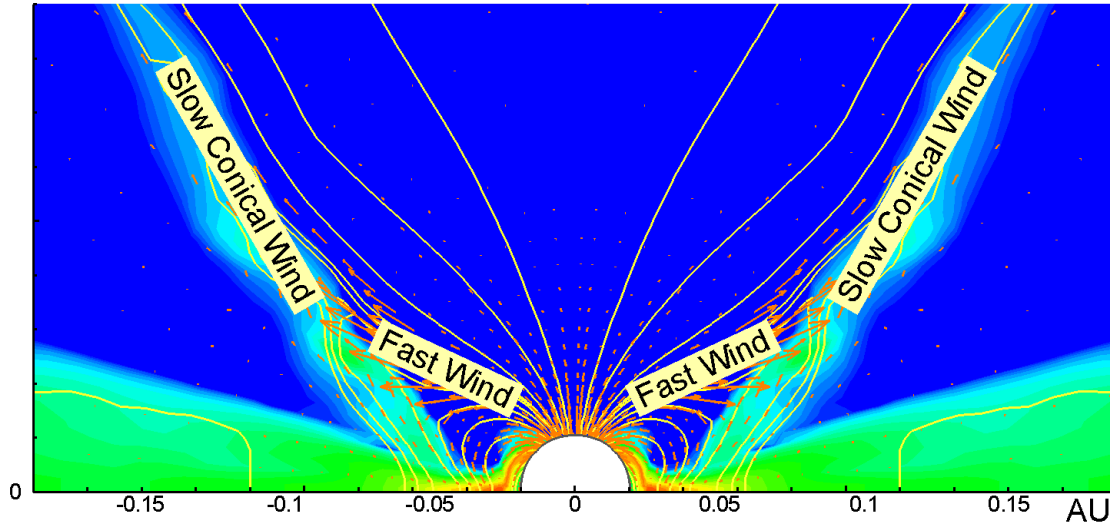


Figure 8. Two components of winds from slowly rotating star are labeled.

celerated and forms a hollow conical wind. At the same time low-density matter is accelerated up to high velocities (hundreds of km/s in CTTSs case) along the inner surface of the cone (i.e., closer to the axis). This high-velocity component may be important in explanation of some highly blue-shifted spectral lines which form near CTTSs (Edward et al. 2003; 2006). Matter which is accelerated in this region may come from the star and/or be captured from the main accretion flow.

The Fig. 2 shows that the conical winds form and later become self-supported for a long time. Figure shows that all magnetic flux which threaded the disk at $T = 0$ is bunched later by the disk into X-type configuration. The inward motion of the disk is slow: it took about $T = 100$ rotational

periods \tilde{P}_0 (at $r = 1$) to reach the vicinity of the star. The outflows started at time $T \approx 150$ and continued for many hundreds of rotations. The magnetic field in the conical winds reconnects frequently and matter is expelled to conical winds in blobs with time-scale about $(5 - 6)\tilde{P}_0$ (see animation at <http://www.astro.cornell.edu/~romanova/conical.htm>).

The Fig. 1 shows conical outflows at one moment of time $T = 500$. The figure also shows velocity vectors of the flow. Most of the matter is accelerated along conical winds. Some low-density matter is accelerated to much higher velocities on the inner side of the cone.

The Fig. 3 shows the distribution of different parameters as a background at time $T = 500$ in the whole region (top) and in the inner part of the region (bottom). The middle pan-

els show the distribution of angular velocity Ω and lines of magnetic flux. One can see that the inner region of the closed magnetosphere rotates with the angular velocity of the star ($1.2 < r < 2$), while the outer region of the corona above the disk (at $r > 2$) rotates with the angular velocity of the disk. The field lines which start at the disk go through the regions of decreasing angular velocity and thus they are strongly wound up owing to the difference in the angular rotation rates. This leads to strong poloidal current rB_ϕ above the disk (see next panels to the right) and the magnetic force associated with gradient of magnetic pressure, $F_m \sim -grad[(rB_\phi)^2]$ appears. This is the main force driving matter to conical winds (as proposed by Lovelace et al. 1991). The right-hand panels (with entropy as a background) show that matter flowing to conical winds is cold.

The Fig. 4 shows the projection of the different forces onto a field line (shown in bold on the bottom panels of Fig. 3). This is one of the field lines which crosses the region where matter is accelerated to conical winds so that we calculate projection of forces to this line starting from the disk and approximately half-way to the star (before it bends towards the star). The Fig. 4 shows that both, centrifugal C and gravitational G forces are large and approximately compensate each other. The centrifugal force is smaller, because a star rotates slowly, so that the sum $G + C$ is negative. The pressure gradient force P is positive inside and near the disk, but it is only strong enough to compensate negative value of $G + C$. The magnetic force M is the main one acting in the positive direction and accelerating matter to conical winds. The gradient of this force is directed approximately in the z -direction, and matter is pushed vertically up. However, it is stopped by the magnetic flux of the dipole and is redirected into a cone. This is why the hollow conical flow is relatively thin and has a relatively small half-opening angle. If the centrifugal force were dominate (as in X-winds, Shu et al. 1994), then the cone would have larger opening angle, and it would not be so narrow, because the centrifugal force has horizontal direction. In addition, the vertical direction of the magnetic force leads to frequent forced reconnection of the magnetic flux threading the conical flows.

The right-hand panels of Fig. 4 show the velocity variation along the same magnetic field line. One can see that the total velocity v_{tot} is almost solely determined by the azimuthal rotation of the flow in the conical wind. Matter is accelerated in the poloidal direction from $\sim c_s$ (near the disk) up to slow magnetosonic v_{sm} , Alfvén v_A and fast magnetosonic v_{fm} velocities. The azimuthal component of velocity v_ϕ is much larger than poloidal component, $v_\phi > 3v_p$. The projection of the poloidal velocity to the chosen field line decreases at larger distances s because the field line curves towards the star. In reality, matter is accelerated more, up to $\sim v \approx 0.5$ in dimensionless units. Note that the sound speed c_s is small so that the pressure gradient is not significant in driving the conical winds.

3.2 Matter and angular momentum fluxes

We calculated the matter fluxes to the star's surface (integrated over $R = 1$), to the conical wind (calculated at $R = 6$), and the matter flux through the disk at $R = 6$. The Fig. 5 (left panels) show matter fluxes. One can see that most of matter incoming in the disk \dot{M}_{disk} accretes to the star, \dot{M}_{star} , while a

smaller part (1/3 in the main case) flows to the conical wind. The bottom panel shows matter flux curves for a small interval of time for better temporal resolution. We also calculated the angular momentum fluxes to the star, to the conical wind, and through the disk.

We calculated the flux of angular momentum through the surface of the star and through the surface $R = 6$. In both cases the flux was calculated as

$$\dot{L} = \int d\mathbf{S} \cdot r \sin \theta \left[\rho v_\phi \mathbf{v}_p - \frac{B_\phi \mathbf{B}_p}{4\pi} - \nu_t \rho r \sin \theta \nabla \omega \right],$$

where $d\mathbf{S}$ is the surface element directed outward to the region. The first term on the right-hand-side \mathbf{L} gives the transport of angular momentum by the matter; the second term is magnetic field contribution; and the third term is the transport due to viscous stress. We also calculated the density of the angular momentum flux and show it as a background in the Fig. 6.

The Fig. 5 (right panels) shows that the largest flux is the inward flux carried by the disk. Only small part ($\approx 1/3$) of this flux is carried away by conical winds. Another small part ($\approx 1/4$) is transported to the (slowly rotating) star mainly through magnetic interaction with much smaller portion transported by the matter. The rest of the flux is transported back by viscous stresses.

The Fig. 6 shows angular momentum flow. The left panel shows that angular momentum to the star is transported by magnetic field. Most of transport occurs through magnetic field lines in the area of the funnel stream, where most of matter flows (see also Romanova et al. 2002; Bessolaz et al. 2007). One can see that the magnetic stress is also high at the base of the conical outflows which means that it is responsible for transport of the angular momentum at the base of the conical winds. Middle panel shows that later, above the disk, angular momentum is carried by matter. Right panel shows angular momentum carried by viscous stress.

3.3 Application to CTTs

CTTs are strongly variable on different time-scales including a multi-year scale (Herbst et al. 2004; Grankin et al. 2007). This is connected with variation of the accretion rate through the disk which may lead to the enhancement of outflows (e.g., Cabrit et al. 1990). Simulations have shown that the bunching of field lines by the new matter after period of the low accretion may lead to quite long outburst of matter to conical winds and may be the reason for formation of micro-jets in the CTTs. If CTT is in a binary system, then an accretion rate may be episodically enhanced due to interaction with the secondary star. Events of fast, impulsive accretion are possible due to thermal instability or global magnetic instability, where the accretion rate is enhanced due to the formation of disk winds (Lovelace et al. 1994). Fig. 7 shows an example of conical winds in case of CTTs. Some observations confirm a hollow cone shape of the outflows from CTTs. For example comparison of possible geometries of outflows observed in H_β line in RW Aurigae led to the conclusion that a conical shaped wind with half-opening angle $30 - 40^\circ$ and a narrow annulus gives the best match to the observations of this line (from Alencar et al. 2005; see Fig. 9).

Two components of the outflow are observed (see Fig. 8) - a slow component, associated with the conical wind, and a

fast component associated with accelerated low-density matter closer to the rotating axis. This high-velocity component may be important in understanding some highly blue-shifted spectral lines which form near CTTSs. Matter which is accelerated in this region may come from the star or it may be captured from the main accretion flow. Observations show that a significant number of CTTS show signs of outflows in spectral lines, in particular in He I (Edwards et al. 2006; Kwan, Edwards, & Fischer 2007).

If CTTS typically in rotational equilibrium state (e.g. Long et al. 2005), then the stars will oscillate between periods of accretion and periods of propeller-driven outflows. In the propeller stage the high velocity component of the outflow is even stronger (see §5).

3.4 Periods of enhanced accretion and outflows in EXors

A period of enhanced accretion may lead to outbursts in EXors, where the accretion rate increases up to $10^{-6} - 10^{-5} M_{\odot}/\text{yr}$ and strong outflows are observed. Brittain et al. (2007) reported on the outflow of warm gas from the inner disk around EXor V1647 observed in the blue absorption of the CO line during the decline of the EXor activity. He concluded that this outflow is a continuation of activity associated with early enhanced accretion and bunching of magnetic field lines (see Fig. 10).

Our simulations are directly applicable to such a situation: new matter comes after period of low accretion rate in CTTS and magnetic field lines are bunched close to the star. The accretion rates are higher than in CTTSs so that all dimensional parameters will correspond to stronger outflows. In our main example of a CTTS, the disk stops at $R_m = 2.4R_*$. In EXors, we take the radius of a star at the Fig. 7 equal to the inner boundary, so that the disk stops much closer to the star, $R_m = 1.2R_*$. Then all velocities are a factor 1.4 higher and densities a factor of 32 higher (compared to Fig. 7), and the matter flux in Fig. 5 is a factor of 11 higher than in the main example relevant to CTTSs.

3.5 Comparison of the model with outflows from the Circinus X-1 - the neutron star hosting binary

Circinus X-1 represents a case where jets are seen from the vicinity of the accreting neutron star. The system is unusual in the sense that Type I X-ray bursts as well as twin-peak X-ray QPOs are observed. The neutron star is estimated to have a weak magnetic field (Boutloukos et al. 2006). The binary system in this case has a high eccentricity ($e \sim 0.4 - 0.9$) and thus has periods of low and high accretion rates (e.g., Murdin 1980). Two-component outflows are observed. The radio observations show a non-stationary jet on both arcmin and arcsecond scales, which appears to have a small opening angle. Recent spectroscopic observations in optics (Jonker et al. 2007) and in X-ray band (Iaria et al. 2008; Schulz et al. 2008) have shown that outflows have a conical structure with a half-opening angle, about 30° . Different explanations are possible for such a conical structure, such as precession of a jet (Iaria et al. 2008). However, this appears less likely because the axis of the jet did not change in 10 years (Tudose et al. 2008). In our understanding this neutron star is a good candidate for

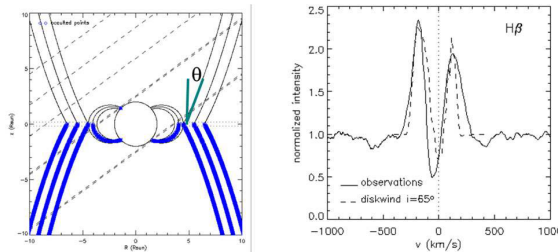


Figure 9. Modeling of the $H\beta$ line in RW Aurigae led to the conclusion that a conical shaped wind with half-opening angle $30 - 40^\circ$ and a narrow annulus gives the best match to the observations of this line (from Alencar et al. 2005).

conical outflows, because (1) it has episodes of very low and very high accretion rates, which is very favorable for formation of conical outflows, (2) a neutron star has only weak magnetic field which can be strongly compressed almost to the stellar surface by the disk which is favorable for conical outflows. This also means that velocity of outflows are of the order of the Keplerian velocity at the surface of the neutron star.

3.6 Application to black hole hosting systems

Jets and winds are observed from accreting black holes including both, stellar-mass black holes and black holes in galactic nuclei. The correlation between enhanced accretion rate and outflows has been extensively discussed and observational data are in favor of this correlation. On the other hand the possibility of magnetic flux accumulation in the inner disk around the black hole and the enhancement it gives to jets has been discussed and observed in numerical simulations (Lovelace et al. 1994; Meier 2005; Igumenshchev 2008). In this situation periods of enhancement of the accretion rate may also lead to bunching of the field lines into an X-type configuration (near the inner radius of the disk) and to formation of conical winds, because the mechanism of conical winds does not require the dipole or any other special configuration. Similarly, the magnetic field of a star may be more complex than a dipole one (see e.g., Donati et al. 2006; Mohanty and Shu 2008).

4 OUTFLOWS IN THE “PROPELLER” REGIME

In case of accreting magnetized stars outflows may be associated with “propeller” stage of evolution (e.g., Illarionov & Sunyaev 1975; Alpar & Shaham 1985; Lovelace et al. 1999) if a star rotates sufficiently fast. At propeller stage fast rotating magnetosphere transfers its angular momentum to the disk matter (e.g. Lovelace et al. 1999). Simulations show that most of matter flows from the inner parts of the disk to widely open cones (Romanova et al. 2005; Ustyugova et al. 2006). The process is quasi-periodic, or episodic (with no definite period) which is connected with opening and closing of magnetic field lines connecting a star and the disk. Such quasi-periodic reconstruction of the magnetosphere due to inflation and reconnection has been predicted theoretically (Aly & Kuipers 1990, Uzdensky, Litwin & Königl 2003) and has been observed in a number of axisymmetric simulations (Hirose

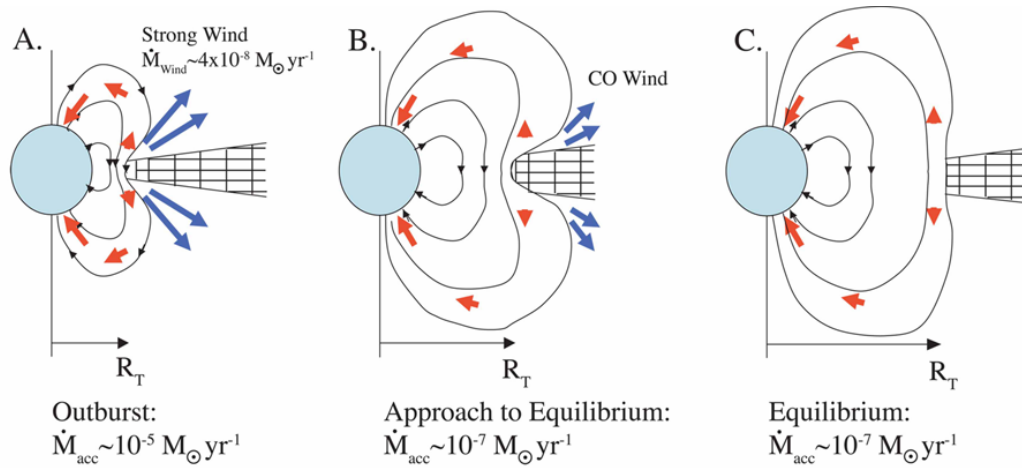


Figure 10. Schematic model of an Exor V1647 Ori. During the outburst the accretion rate is enhanced so that the magnetospheric radius R_m decreases and the magnetic field lines were bunched (A). This results in a fast, hot outflow. As the accretion rate decreases, the disk moves outward and this results in a slower, cooler CO outflow (B). Further decrease in the accretion rate leads to a quiescence state where the production of warm outflows stops (C). From Brittain et al. (2007)

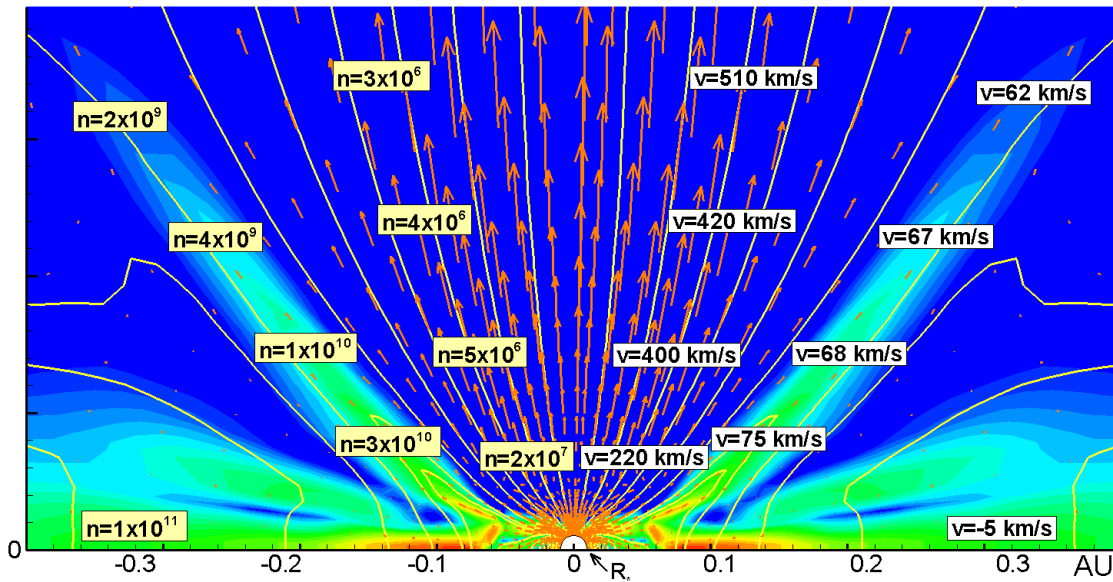


Figure 11. Outflows in the propeller regime. The background shows matter flux, lines are selected field lines, arrows are proportional to velocity. Labels show total velocity and density at sample points.

et al. 1997; Goodson et al. 1997, 1999; Matt et al. 2002; Romanova et al. 2002; von Rekowski & Brandenburg 2004). Multiple events of inflation and reconnection (hundreds of outbursts) were observed in simulations of the propeller stage (Romanova et al. 2005; Ustyugova et al. 2006; see animation at <http://www.astro.cornell.edu/~romanova/propeller.htm>).

In the propeller regime the magnetosphere rotates faster than inner region of the disk. This occurs if the co-rotation radius $R_{cr} = (GM/\Omega_*^2)^{1/3}$ is smaller than magnetospheric radius R_m (e.g., Lovelace et al. 1999). Young stars are expected to be in the propeller regime in two situations: (1) At the early stages of evolution (say, at $T < 10^6$ years), when the star formed but did not have time to spin-down, and (2) at later stages of evolution, such as at CTTS stage, when the star is expected to be on average in the rotational equilibrium

state (e.g., Long et al. 2005) but variation of the accretion rate leads to variation of R_m around R_{cr} , where $R_{cr} < R_m$ is possible. We performed axisymmetric simulations of accretion to a star in the propeller regime, taking a star with the same parameters as in case of conical winds, but with period $P_* = 1$ day (Romanova et al. 2005; Ustyugova et al. 2006). We chose $\alpha_v = 0.3$ and $\alpha_d = 0.1$ and thus bunched the field lines to the X-type configuration. We observed that in addition to conical wind there is a fast axial jet (see Fig. 11) so that the outflow has two components (see Fig. 12). The conical wind in this case is much more powerful - it carries most of the disk matter away. The axial jet carries less mass, but it is accelerated to high velocities. Acceleration occurs due to the magnetic pressure of the “magnetic tower” which forms above the star as a result of winding of magnetic field lines

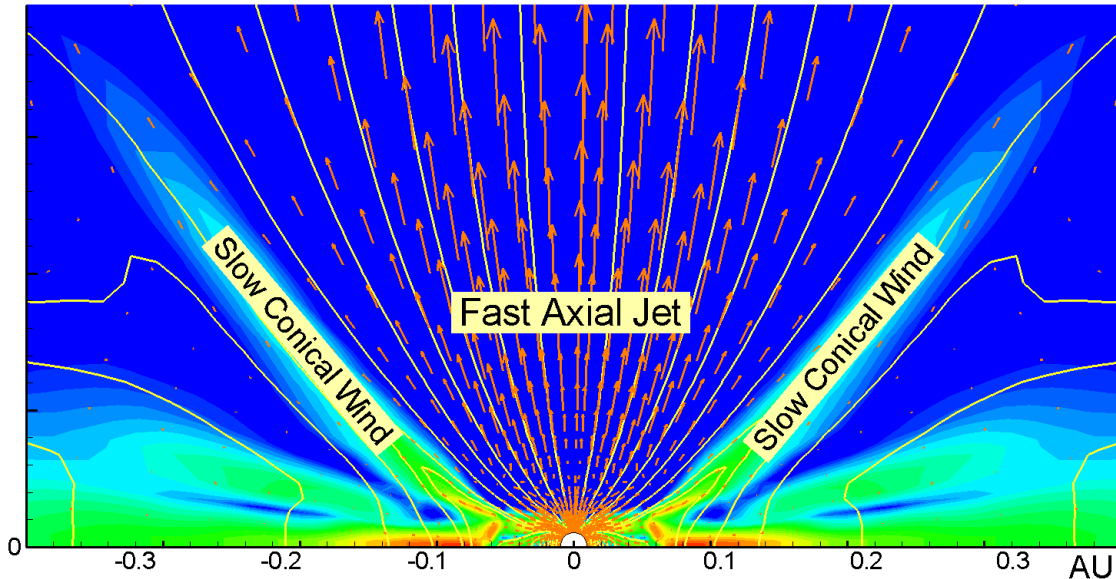


Figure 12. Two components of outflows in the propeller regime.

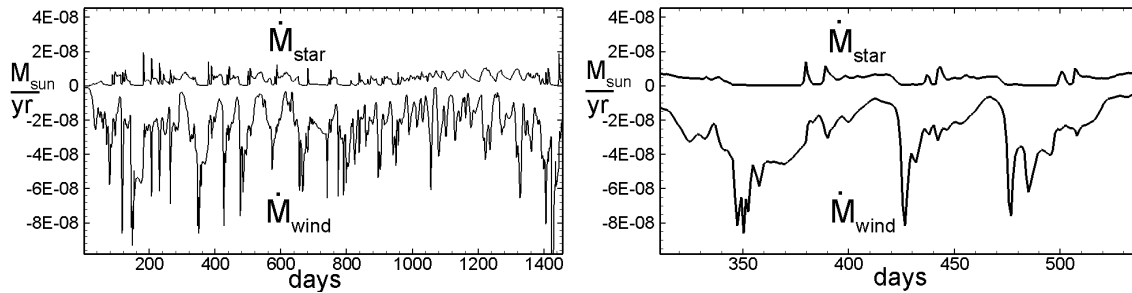


Figure 13. Two components of outflows in the propeller regime.

of the star. Outbursts to conical winds occur sporadically with a long time-scale interval (see Fig. 13) which is connected with the long time-scale interval of accumulation and diffusion of the disk matter through the magnetosphere of the star (see also Goodson et al. 1997; Fendt 2008). These propeller outflows were obtained in conditions favorable for such a process: when the star rotated fast and an X-type configuration developed. Future simulations should be done for the case of propeller-driven outflows from slower rotating CTTS. Collimation of conical winds may occur at larger distances from the star for example, by disk winds (e.g., Königl & Pudritz 2000; Ferreira et al. 2006; Matsakos et al. 2008).

5 3D SIMULATIONS OF CONICAL WINDS

We performed exploratory simulations of conical winds in global 3D simulations. One of main questions is what is an expected direction of conical winds when magnetosphere of the star is misaligned relative to the rotational axis. We chosen a case when magnetosphere of a star is misaligned relative to the rotational axis at an angle $\Theta = 30^\circ$. We took a cubed sphere code developed earlier (Koldoba et al. 2002, Romanova et al. 2003) and used a grid $N_r \times N^2 = 120 \times 51^2$ in each of 6 blocks of the sphere. At such fine grid we were able

to handle the case with the low-density corona $\rho_c = 0.001$ and took the density in the disk $\rho_d = 2$ which is 5 times lower than in the axisymmetric case. However we also took smaller magnetic moment of the star, $\tilde{\mu} = 2$ (compared to $\tilde{\mu} = 10$ in the axisymmetric case), again, to save computing time. We did not push a disk from too large distances (to save computing time) but from $r = 5$ which is far enough to insure an initial bunching of the magnetic field lines. Subsequently, the bunching had been supported by sufficiently high viscosity, $\alpha_{vis} = 0.3$. We do not have diffusivity in the 3D code however at such a grid estimated numerical diffusivity at the disk-magnetosphere boundary is at the level $\alpha_d \sim 0.01 - 0.02$ so that conditions for conical winds are satisfied, that is $Pr_m > 1$.

Simulations have shown that accreting matter bunched field lines and that some matter went to conical winds. Fig. 14 shows that conical winds are geometrically symmetric relative to the rotational axis of the star Ω in the sense that an angle between different parts of the conical winds and Ω axis is approximately the same. However the density distribution in the wind shows a spiral structures in the form of density amplification, which rotates with an angular velocity of the star, Ω_* , and represents a one-arm spiral from each side of the outflow.

Note that at $\alpha_{vis} = 0.3$ the disk-magnetosphere interac-

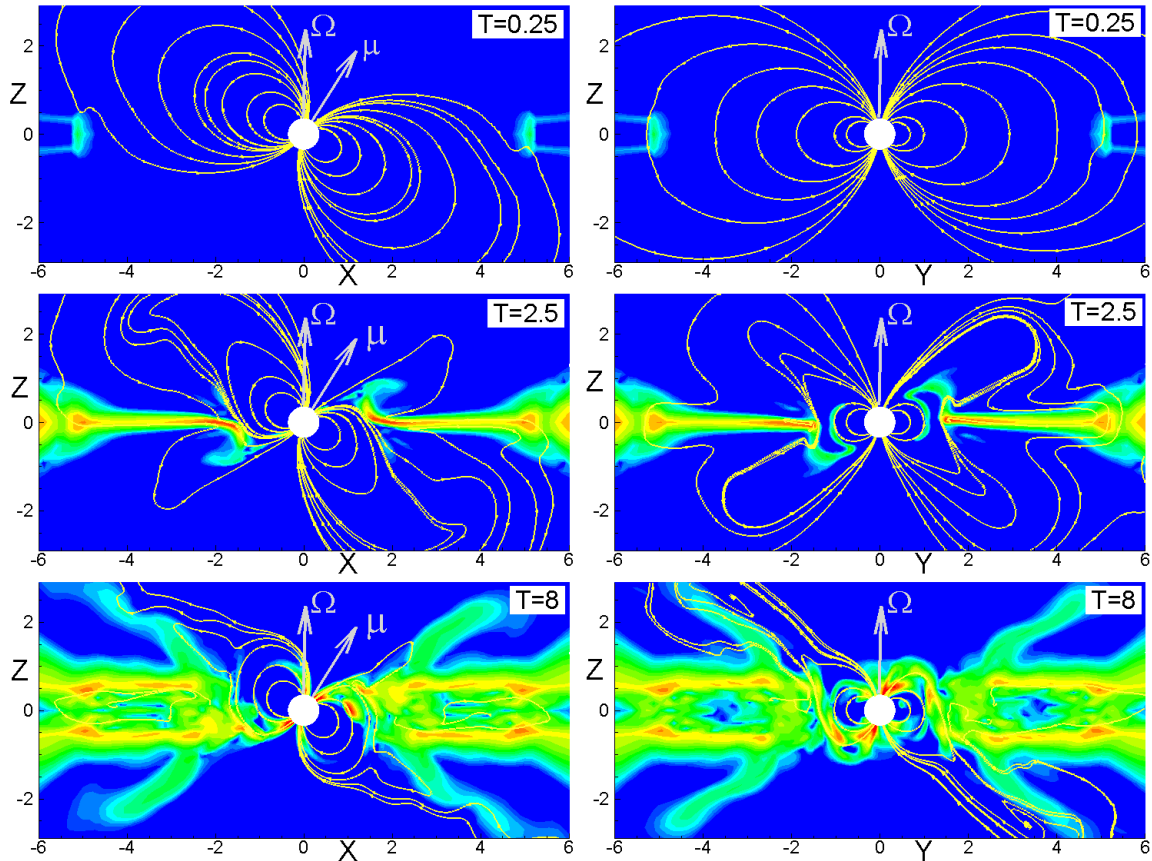


Figure 14. Projections show formation of conical winds obtained in 3D MHD simulations. Left panels show an XZ slice in the distribution of matter flux (background) and magnetic field lines in different moments of time. Right panels show corresponding YZ slices. Arrows show the direction of the magnetic moment of the star μ and angular velocity of rotation Ω .

tion has tendency to be unstable relative to the interchange instability (Romanova, Kulkarni & Lovelace 2008; Kulkarni & Romanova 2008) and we do observe partial accretion through instabilities in addition to funnel stream accretion which dominates at pretty high inclination of the dipole $\Theta = 30^\circ$ (Kulkarni & Romanova 2009). One can see that conical winds start blowing from those parts of the disk which are quite far away from the disk-magnetosphere boundary. We can guess that again, the accumulation of the B_ϕ component above the disk drives matter outward to the conical winds. However we should be caution in giving global conclusion about non-dependence of conical winds from instabilities. Penetration of the inner disk matter through the magnetosphere through instabilities decreases the density at the inner edge of the disk and ability of the disk matter to strongly compress the magnetosphere which is a favorable condition for strong conical winds. This possible interrelation between instabilities and conical outflows should be checked in the future 3D simulations in greater detail.

6 INVESTIGATION OF PARAMETER RANGE

To investigate the dependence on different parameters we took the main case and varied one parameter at a time. The main effort has been directed at understanding the dependence on the effective viscosity and the effective magnetic

diffusivity. We performed two sets of runs: (1) at fixed diffusivity and different viscosity coefficients, and (2) at fixed viscosity and different diffusivity coefficients.

Dependence on viscosity at fixed diffusivity. We fixed the diffusivity at $\alpha_{dif} = 0.1$ and varied the viscosity coefficient in the range $\alpha_{vis} = 0.01 - 1$. We observed that for small viscosity, $\alpha_{vis} < 0.1$, the magnetic field of the dipole diffuses through the inner regions of the incoming disk and an X-type configuration does not form. No conical outflows appear in this case. We conclude that formation of conical winds requires $\alpha_{vis} > \alpha_{dif}$, that is, $Pr_m > 1$. Next we increased α_{vis} and observed that the X-type configuration formed and conical outflows were generated. We observed that the accretion rate to the star strongly increases with α_{vis} , while outflow rate to the conical winds increases but only slowly. For $\alpha_{vis} = 0.1$, the matter fluxes to the star and to the wind are small and approximately equal. For $\alpha_{vis} = 0.3$ and 0.4 , the wind carries about 30% and 20% of mass correspondingly). Angular momentum carried to the star also strongly increases with α_{vis} . In all cases the star spins-up, because the magnetospheric radius, $r_m \approx 1.2$ is smaller than corotation radius which is $r_{cor} = 3$. That is, incoming matter brings positive angular momentum to the star. Conical outflows carry angular momentum away from the disk. We should remember however that it is only a small part of the total angular momentum of the disk as shown above. For $\alpha_{vis} = 0.3$ and 0.4 , matter outflows to the conical winds in oscillatory fashion. We often

observe that quasi-periodic oscillations of the accretion occur for $Pr_m \approx 3 - 4$.

Dependence on diffusivity at fixed viscosity. In the next set of runs we fixed the viscosity at $\alpha_{vis} = 0.3$ and varied the diffusivity: from 0.01 to 1. Again, no conical winds were formed for $\alpha_{dif} > \alpha_{vis}$. At relatively high diffusivity, $\alpha_{dif} = 0.1, 0.3$, about 30% of the incoming matter flows to the conical winds. For $\alpha_{dif} = 0.1$ ($Pr_m = 3$) conical outflows oscillate, while at $\alpha_{dif} = 0.3$ ($Pr_m = 1$) no oscillations are observed. For very small diffusivity, $\alpha_{dif} = 0.01$, the conical outflows also form with slightly smaller matter flux to the winds. However, the accretion rate to the star is larger. This is somewhat unexpected because one would expect that at small α_{dif} matter of the disk would be trapped by strong magnetic flux accumulated at the inner edge of the disk. The possible explanation may be that penetration of matter of the disk through the disk-magnetosphere boundary is determined by the local Reynolds number $Re_m = \Delta r v_r / \eta_m$, which is determined not only by the diffusivity coefficient $\eta_m \sim \alpha_{dif}$, but also by the velocity of the flow, v_r , which become very small at the disk-magnetosphere boundary, and also by the size Δ_r of the boundary, which also become very small at high Prandtl numbers. Angular momentum fluxes to the star and to the winds are approximately the same, excluding the case $\alpha_{dif} = 0.01$ where the flux to the star is larger. This approximate equality *does not* mean that the conical winds carry angular momentum flux out of the star. Instead, they carry angular momentum from the inner regions of the disk. The remaining angular momentum of the disk goes to the spinning-up the star and part of the angular momentum of the disk flows outward in the disk due to the viscous stress.

Variation of other parameters. We varied the *period of the star (corotation radius)* taking $r_{cor} = 5, 10$ for slowly rotating stars and $r_{cor} = 1.5, 2$ - for faster rotating stars. In the case of slowly rotating stars conical winds form and the outflow rate to the winds is similar to one in the main case for $r_{cor} = 3$, though accretion rate to the star is somewhat larger. For faster rotating star, $r_{cor} = 2$, the amplitude of variability increased and matter flux to outflows increased up to 50%–70% compared to the accretion rate to the star. For even faster rotation, $r_{cor} = 1.5$, the accretion rate decreased by a factor of 5 compared to the main case, while the outflow to conical winds increased by a factor of 2. Thus most of matter is ejected to conical winds. This situation become close to the propeller regime, where the corotation radius becomes close to the magnetospheric radius, $r_m \approx 1.2$ where most of the incoming matter may be ejected to the outflows (Lovelace et al. 1999; Romanova et al. 2005; Ustyugova et al. 2006).

Outflow of matter to winds occurs if the corona is not very dense so that outflowing matter of the winds does not lose its energy while propagating through the corona. In the main simulation runs an initial density of the corona is 10^{-4} times the disk density ($\rho_d = 10$ versus $\rho_c = 10^{-3}$). To test the dependence on the coronal density we decreased its density by a factor of 3 and first chose smaller (compared to the main case) transport coefficients, $\alpha_{vis} = 0.1, \alpha_{dif} = 0.03$, hoping to enhance outflows to the winds. Simulations have shown that matter fluxes to the star and to the winds are not appreciably different from the main case. We conclude that the coronal density used in the main case is sufficiently small as to not suppress the outflows.

Summarizing the above subsections we conclude that:

- (1) **Strong conical outflows** appear at a wide range of parameters if both the magnetic viscosity and diffusivity are not very small, $\alpha_v > 0.1$ and $\alpha_d > 0.01$. Outflows are most powerful when the viscosity is a few times larger than diffusivity. For these parameters the viscosity is high enough to drive disk matter inward to the region of stronger magnetic field, while the diffusivity is high enough to ensure the penetration of disk matter through the bunched field lines.
- (2) **Weak outflows** are observed when the viscosity is large and the diffusivity is very small. In this case the field lines are bunched into the X-type configuration. However, the diffusivity is not high enough to ensure loading of the disk matter to the field lines of the magnetosphere.
- (3) **Slow accretion, no outflows** occurs when the viscosity is small, $\alpha_v < 0.1$ for any value of the diffusivity α_d . In this case the disk is stopped at larger distances from the star by the strong magnetic field of the star. Only very weak outflows or no outflows are observed in this case.

7 CONCLUSIONS

We discovered a new type of outflows - hollow conical winds - in MHD simulations of disk accretion to a rotating magnetized star. The conical winds occur under conditions where the poloidal magnetic field is bunched into an X-type configuration.

In some respects these winds are similar to the X-winds proposed by Shu and collaborators (e.g., Shu et al. 1994):

1. They both require bunching of the field lines;
2. They both have high rotation of the order of Keplerian rotation at the base of outflow, and gradual poloidal acceleration;
3. They both are driven by the magnetic force (see also Lovelace et al. 1991).

However, there are a number of important differences:

1. Conical winds flow in a thin shell (they are hollow), while X-winds flow at different angles below the “dead zone”;
 2. Conical winds form around stars of any rotation rate including slow rotation, and do not require the fine tuning of angular velocity of the inner disk to that of magnetosphere;
 3. Conical winds are non-stationary: the magnetic field constantly inflates and reconnects;
 4. Conical winds carry away part of the angular momentum of the inner disk and are not responsible for spinning-down the star, while X-winds are predicted to take away angular momentum from the star;
 5. In the conical winds there is a fast component of the flow along field lines threading the star.
 6. In the propeller regime (where the corotation radius is comparable or smaller than magnetospheric radius) a new component appears: a strong magnetically dominated jet along the open field lines of the star. In this component low density matter is accelerated up to super-Keplerian velocities. The star loses its angular momentum mainly due to the twisted magnetic field of this component.
- Some of these differences, such as non-stationarity of conical winds is connected with natural restrictions of the stationary model of X-winds.

Conical winds can explain the hollow conical shape of outflows near young stars of different type (CTTSs, EXors, Type I objects) which have been recently resolved. The conical winds may arise from any type of the disk-accreting magnetized stars, including accreting young stars, white dwarfs, neutron stars and possibly black holes as mentioned. An exact configuration of the magnetic flux is not important: only the bunching/inclination and inflation of the flux are important. This makes this mechanism universal and it may work in different situations. It is often observed that enhancement of the accretion rates leads to enhanced outflows. Mechanism of conical winds gives natural explanation of such events observed in a wide variety of astrophysical objects.

It is still not known what are the values of transport coefficients in real accretion disks. MRI simulations have shown that magneto-rotational mechanism of turbulent transport may give values of α in the range: $\alpha_{vis} = 10^{-2} - 0.4$ (e.g., Stone et al. 2000) and corresponding diffusivity values. If in real disks transport coefficients are large, $\alpha \sim 0.1$ then strong outflows are expected during periods when $\alpha_{vis} > \alpha_{dif}$ with steady flow to the wind or with short-period variability like in Fig. 5. If in the opposite case the transport coefficients are always small, say $\alpha_{vis} = \alpha_{dif} = 0.01$, then conical outflows are expected only during periods of enhanced accretion when accretion rate is enhanced due to e.g. some instabilities or other mechanism of angular momentum transport, e.g., Rossby waves (Lovelace et al. 1999; Li et al. 2000). Then outflows will be characterized by high-amplitude outbursts to conical winds with a large time-interval between outbursts determined by the small diffusivity at the disk-magnetosphere boundary (similar to that in the propeller regime (e.g., Fig. 13).

If a star is in the propeller regime, then clear two-component outflows are observed:

(1) Conical-type winds which may carry away significant part of the *disk mass and angular momentum*, with velocities approximately equal to Keplerian velocity at the base of the winds.

(2) Magnetically dominated axial jet where low-density matter is accelerated near the star to much higher velocities. The twisted magnetic field of this jet carries away most of the angular momentum of the star.

The propeller regime may be responsible for the fast loss of angular momentum by young stars before their CTTS stage. It may also appear in stars which are in rotational equilibrium during periods of the accretion rate is lower.

The propeller-driven axial jet has good collimation due to interaction with surrounding conical wind. The overall conical wind may be collimated at larger distances by disk winds emanating from the disk at large radii (Blandford & Payne 1982) or the pressure of the external medium (Lovelace et al. 1991). Typical terminal velocity of outflows from the disk are of the order of the Keplerian velocity at the radius from which matter flows to the wind and is expected to be smaller than velocity in conical winds, though the total angular momentum may be larger (e.g., Ferreira et al. 2006).

ACKNOWLEDGMENTS

The authors thank S. Edwards, S. Cabrit, E. Dougados, J. Ferreira and F. Shu for helpful discussions. The authors were supported in part by NASA grant NNX08AH25G and by NSF grants AST-0607135 and AST-0807129. MMR thanks NASA for use of the NASA High Performance Facilities. AVK and GVU were supported in part by grant RFBR 06-02016608, Program 4 of RAS.

REFERENCES

Alencar, S. H. P., Basri, G., Hartmann, L., Calvet, N. 2005 A&A, 440, 595
 Alpar, M.A., & Shaham, J. 1985, Nature, 316, 239
 Aly, J.J., & Kuijpers, J. 1990, A&A, 227, 473
 Bacciotti, F., Mundt, R., Ray, T.P., Eisloffel, J., Solf, J., Camezind, M. 2000, ApJ, 537, L49
 Bessolaz, N., Zanni, C., Ferreira, J., Keppens, R., Bouvier, J. 2008, A&A, 478, 155
 Blandford, R.D., & Payne, D.G. 1982, MNRAS, 199, 883
 Boutloukos S., van der Klis M., Altamirano D., Klein-Wolt M., Wijnands R., Jonker P.G., Fender R.P., 2006, ApJ, 653, 1435
 Brittain, S., Simon, T., Rettig, T.W., et al. 2007, Star-Disk Interaction in Young Stars, IAU Symposium No. 243, ed. J. Bouvier & I. Appenzeller, p. 223
 Cabrit, S., Edwards, S., Strom, S.E., & Strom, K.M. 1990, ApJ, 354, 687
 Cai, M.J., Shang, H., Lin, H.-H., & Shu, F.H. 2008, ApJ, 672, 489
 Donati, J.-F., Forveille, T., Cameron, A.C., Barnes, J.R., Delfosse, X., Jardine, M.M., & Valenti, J.A. 2006, Science, 311, 633
 Edwards, S., Fischer, W., Hillenbrand, L., Kwan, J. 2006, ApJ, 646, 319
 Edwards, S., Fischer, W., Kwan, J., Hillenbrandt, L., Durpee, A.K. 2003, 599, L41
 Fendt, C. 2008, astro-ph: arXiv:0810.4154v1
 Ferreira, J, Dougados, C., & Cabrit, S. 2006, A&A, 453, 785
 Goodson, A.P., Winglee, R. M., & Böhm, K.-H. 1997, ApJ, 489, 199
 Goodson, A.P., Böhm, K.-H., Winglee, R. M. 1999, ApJ, 524, 142
 Grankin, K. N., Melnikov, S. Yu., Bouvier, J., Herbst, W., Shevchenko, V. S. 2007, A&A, 461, 183
 Heinz, S., Schulz, N. S., Brandt, W. N., & Galloway, D. K. 2007, ApJ, 663, L93
 Herbst, W., Herbst, D. K., Grossman, E. J., Weinstein, D. 2004, AJ, 108, 1906
 Iaria R., D’Aí A, Lavagetto G., Di Salvo T., Robba N.R., Burderi L., 2008, ApJ, 673, 1033
 Igumenshchev, I.V. 2008 ApJ, 677, 317
 Illarionov, A.F., & Sunyaev, R.A. 1975, A&A, 39, 185
 Jonker, P.G., Nelemans, G., Bassa, C.G. 2007, MNRAS, 374, 999
 Konigl, A., & Pudritz, R. E. 2000, Protostars and Planets IV, Mannings, V., Boss, A.P., Russell, S. S. (eds.), University of Arizona Press, Tucson, p. 759
 Kulkarni, A., & Romanova, M.M. 2008, MNRAS, 386, 673
 Kwan, J., Edwards, S., & Fischer, W. 2007, ApJ, 657, 897
 Li, H., Finn, J.M., Lovelace, R.V.E., & Colgate, S.A. 2000, ApJ, 533, 1023

- Livio, M. 1997, *Accretion Phenomena and Related Outflows*; IAU Colloquium 163. ASP Conference Series; Vol. 121; ed. D. T. Wickramasinghe; G. V. Bicknell; and L. Ferrario, p.845
- Long, M., Romanova, M. M., & Lovelace, R. V. E. 2005, *ApJ*, 634, 1214
- Lovelace, R.V.E., Berk, H.L., & Contopoulos, J. 1991, *ApJ*, 379, 696
- Lovelace, R.V.E., Li, H., Colgate, S.A., & Nelson, A.F. 1999, *ApJ*, 513, 805
- Lovelace, R.V.E., Romanova, M.M., & Bisnovatyi-Kogan, G.S. 1999, *ApJ*, 514, 368
- Lovelace, R.V.E., Romanova, M.M., & Newman, W.I. 1994, *ApJ*, 437, 136
- Matsakos, T., Tsinganos, K., Vlahakis, N., Massaglia, S., Mignone, A., Trussoni, E. 2008, *A&A*, 477, 521
- Matt, S., Goodson, A.P., Winglee, R.M., & Böhm, K.-H. 2002, *ApJ*, 574, 232
- Meier, D.L. 2005, *Ap&SS*, 300, 55
- Mohanty, S., & Shu, F.H. 2008, *ApJ*, in press (arXiv:0806.4769)
- Murdin P., Jauncey D.L., Haynes R.F., Lerche I., Nicolson G.D., Holt S.S., Kaluzienski L.J., 1980, *A&A*, 87, 292
- Najita, J.R., & Shu, F.H. 1994, *ApJ*, 429, 808
- Pyo, T.-S., Hayashi, M., Kobayashi, N. et al. 2003, *ApJ*, 649, 836
- Ray, T., Dougados, C., Bacciotti, F., Eislffel, J., & Chrysostomou, A. 2007, *Protostars and Planets V*, B. Reipurth, D. Jewitt, and K. Keil (eds.), University of Arizona Press, Tucson, p. 231
- Romanova, M.M., Kulkarni, A.K., & Lovelace, R.V.E. 2008, *ApJ*, 673, L171
- Romanova, M.M., Ustyugova, G.V., Koldoba, A.V., & Lovelace, R.V.E. 2002, *ApJ*, 578, 420 (RUKL)
- Romanova, M.M., Ustyugova, G.V., Koldoba, A.V., & Lovelace, R.V.E. 2005, *ApJ*, 635, 165L
- Romanova, M.M., Long, M., Kulkarni, A. K., Kurosawa, R., Ustyugova, G.V., Koldoba, A.K., & Lovelace, R.V.E. 2007a, in *IAU Symp.*, Vol. 243, *Star-Disk Interaction in Young Stars*, ed. J. Bouvier & I. Appenzeller, “*MHD Simulations of Disk-star Interaction*”
- Shakura, N.I., & Sunyaev, R.A. 1973, *A&A*, 24, 337
- Shu, F., Najita, J., Ostriker, E., Wilkin, F., Ruden, S., Lizano, S. 1994, *ApJ*, 429, 781
- Shu, F.H, Galli, D., Lizano, S., Glassgold, A.E., & Diamond, P.H. 2007, *ApJ*, 665, 535
- Stone, J. M., Gammie, C. F., Balbus, S. A., & Hawley, J. F. 2000, *Protostars and Planets IV* (Book - Tucson: University of Arizona Press; eds Mannings, V., Boss, A.P., Russell, S. S.), p. 589
- Sokoloski, J.L., & Kenyon, S.J. 2003, *ApJ*, 584, 1021
- Takami, M., Beck, T.L., Pyo, T.-S., McGregor, P., Davis, C. 2007, *ApJ*, 670, L33
- Tudose, V., Fender, R. P., Tzioumis, A. K., Spencer, R. E., & van der Klis, M. 2008, *MNRAS*, 390, 447
- von Rekowski, B., & Brandenburg, A. 2004, *A & A*, 420, 17
- Ustyugova, G.V., Koldoba, A.V., Romanova, M.M., & Lovelace, R.V.E. 1999, *ApJ*, 516, 221
- Ustyugova, G.V., Koldoba, A.V., Romanova, M.M., & Lovelace, R.V.E. 2006, *ApJ*, 646, 304